Electronic Supplementary Material (ESI) for Soft Matter.

Supporting Information

Poroelasticity of highly confined hydrogel films measured with a surface forces apparatus

George D. Degen,*[a] Jonathan Chen,[a] Allison L. Chau,[b] Lisa K. Månsson[c] and Angela A. Pitenis[b]

[a]Department of Chemical Engineering, University of California, Santa Barbara, Santa Barbara, CA 93106, USA. E-mail: gdegen@ucsb.edu

[b]Materials Department, University of California, Santa Barbara, Santa Barbara, CA 93106, USA.

[c]Department of Physics, Chalmers University of Technology, SE-412 96 Gothenburg, Sweden

S1. Hydrogel film preparation and confocal microscopy 2
  Figure S1. Confocal microscopy of gel films 3
S2. Distance and force measurements 3
  Figure S2. SFA Schematic and force calculation 5
S3. Crossed cylinder force derivation 5
S4. Theoretical estimation of permeability 6
S5. Poroelastic model and algorithm for force calculation 6
  Figure S3. Compressions of gels of different thicknesses 7
  Figure S4. 20- and 60-min relaxation plots 8
  Figure S5. Hydrogel film after addition of 100% ethanol 8
  Figure S6. Hydrogel swelling ratios in ethanol solutions 9
  Figure S7. Viscosity of ethanol/water solution 10
S6. References 10

S1. Hydrogel film preparation and confocal microscopy

A layer of silver (thickness 46-50 nm) was deposited onto two cylindrical glass disks (radius of curvature $R = 2$ cm) via thermal evaporation. Gels of thickness 32 and 68 µm were cast directly on the silver surface. For the gel film of thickness 11 µm, additional surface preparation was used to prevent wrinkling during swelling. One of the silvered disks was functionalized with a cysteamine monolayer[1] via immersion in a 20mM aqueous cysteamine (Sigma-Aldrich) solution for 5 min. The concentration and incubation time were chosen to enable sufficient coverage of cysteamine[2] but avoid dissolution of the silver film. The surface was rinsed with ultrapure water (Millipore), then immersed in a 5 wt% aqueous glutaraldehyde (Sigma-Aldrich) solution for 5 min to covalently attach glutaraldehyde to the cysteamine monolayer,[3] and finally immersed in ultrapure water for 5 min.

To cast the hydrogel on cylindrical surfaces, a mold was prepared from two pieces of single-sided tape applied to a freshly cleaved mica strip (~1 x 2.5 cm) forming a channel down the long axis (main text, Figure 1A). Tape thicknesses included 5 µm (Nitto Denko Corporation, UTS-5BSL), 10 µm (Nitto Denko Corporation, UTS-10BAF), and 30 µm (3M Scotch). The tape surfaces were coated with a hydrophobic pen to limit fluid leakage during casting (Daido Sangyo Co. Ltd). Hydrogels were polymerized from the following components in the specified mass ratios: acrylamide monomer (AAm, 7.5%, Sigma-Aldrich), N,N′-methylenebisacrylamide (MBAm, 0.3%, Sigma-Aldrich), N,N,N′,N′-tetramethylethylenediamine (TEMED, 0.15%, Sigma-Aldrich), ammonium persulfate (APS, 0.15%, Sigma-Aldrich), and ultrapure water. Special care was taken when handling the toxic acrylamide monomer and when disposing of waste. Immediately after mixing the hydrogel solution, 10 µL was deposited onto the cylinder and compressed with the mold for 5 min. The mold was then removed from the polymerized gel, which was then immersed in ultrapure water for at least 24 h. A new mold was prepared for each film. When preparing the molds, special care was taken to avoid wrinkling of the tape. The 5 µm thick tape was particularly susceptible to wrinkling upon application to the mica, and the presence of wrinkles greatly increased the thickness of the resulting gel film. With careful tape application, gels of swollen volume between 7 and 12 the 5 µm were cast using the 5 µm tape.

To assess film uniformity, 28.5 µL of 0.005 vol% solution of fluorescent beads (Fluoro-Max Red Fluorescent Microspheres, $\lambda_{\text{excitation}} = 542$ nm, $d = 490$ nm) in ultrapure water was mixed with 21.5 µL PAAm solution to yield 50 µL 7.5 wt% PAAm solution. 10 µL of this solution was cast between the bottom of a glass bottom petri dish and a freshly cleaved mica sheet. Strips of 5 µm thick tape (Nitto Denko Corporation, UTS-5BSL) were used as separators. To chemically attach the PAAm to glass, the glass surface was treated with UV/ozone (UVOCS T10x10/OES) for 10 min and then soaked in a 1:20 solution of 3-aminopropyl-triethoxysilane (APTES, 99.7%) in ultrapure water for 5 min. After rinsing with ultrapure water, the glass was soaked in a 1:20 solution of glutaraldehyde (Sigma Aldrich, 50 wt% in H2O) in ultrapure water for 5 min and then rinsed again with ultrapure water. Gels were prepared with and without the glutaraldehyde treatment of the surfaces.

A confocal microscope (Nikon Eclipse Ti2-E, A1R-HD) was used to measure the film thickness. The z-stacks were obtained with a 488 nm laser and step size of 0.5 µm. The polymerized film was analyzed before and after equilibration in water. Equilibration resulted in swelling of the gel, which took less than 5 min. This equilibration time is consistent with the equilibration time predicted by polymer scaling[4]: $t \cong L^2/D$ where L is the characteristic size of the gel and D is the diffusion coefficient. Taking L as the film thickness (~10 µm) and a typical value of diffusion coefficient[4,5] $L = 10^{-11}$ m^2/s yields $t \approx 10$ s. The number of beads per stack was detected utilizing the NIS-Elements software and plotted against z position (Figure S1). Film thickness was determined from the width of the resulting curves.

We note that because the thicker gels were cast directly on the silver surface, they may have wrinkled upon swelling in water. We assumed that wrinkles would be flattened during compression and that after the gel was flattened, the compressive forces would be similar to those of a flat gel. This flattening is expected to result in relatively long-ranged repulsive forces. Since the film thickness was determined by fitting the poroelastic model to the compression forces, these long-ranged forces did not substantially affect the determination of the film thickness, since they accounted for a small percentage of the total forces. However, since the compression depth was calculated using the film thickness, a consequence of the fitting procedure and long-ranged forces is that repulsive forces appear at zero compression depth, as seen for the 32 µm film in Figure 2B in the main text.

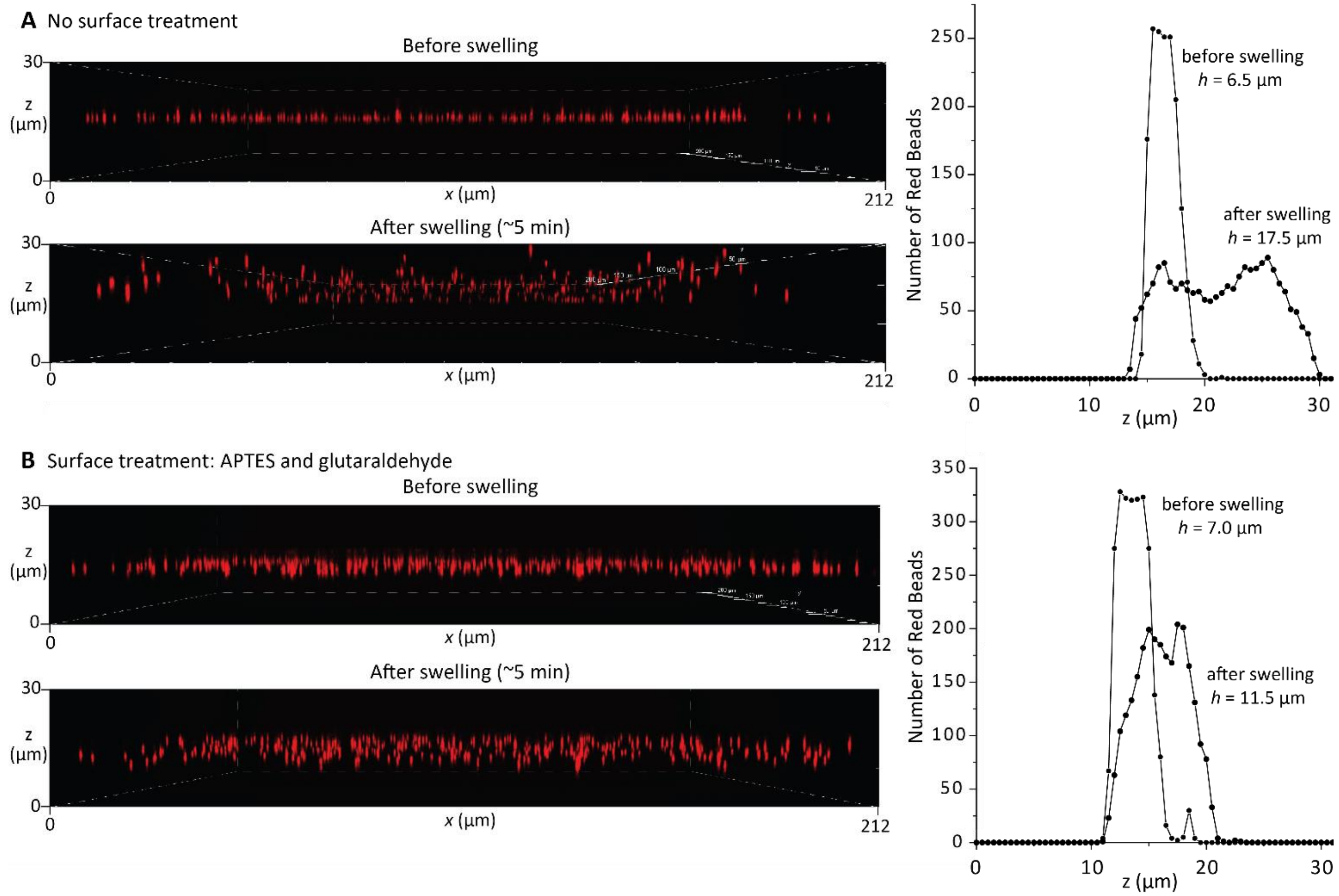

Figure S1. Confocal microscopy of gel films incorporating fluorescent beads. Images show fluorescence as a function of depth z and horizontal position x in the gel film. Plots show the total number of fluorescent beads as a function of z, where the width of the nonzero region corresponds to the film thickness. A) Gels deposited directly on glass show variations in the locations of the fluorescent beads in the z direction, indicating wrinkling of the film. B) Gels deposited on glass functionalized with APTES/glutaraldehyde. The consistent locations of the fluorescent beads in the z direction indicate the gels swell uniformly with minimal wrinkling.

S2. Distance and force measurements

Distance Measurement

In the SFA (SFA2000, SurForce LLC), white light multiple beam interferometry gave the distance D between the silver surfaces as follows. The hydrogel film was compressed between silver layers on each glass cylinder, forming a one-layer interferometer. Following Israelachvili,[6] D is related to the wavelengths of constructive interference λ_{n} and fringe order n by the following

$$D = \frac{n\lambda_{\mathrm{n}}}{2\mu} \tag{S1}$$

The refractive index μ in Equation S1 was equal to the refractive index μ_{gel} of the compressed hydrogel, calculated as a mass weighted average of the polymer refractive index[7] (1.5) and the refractive index of the solution μ_{sol}, which was either the dispersive refractive index of water[8] or non-dispersive refractive index of the ethanol/water solution.[9] We ignore the phase change at the silver-gel interface and dispersion of the polymer and ethanol/water solutions. The fringe order is calculated from the wavelengths of adjacent fringes as follows:

$$\frac{1}{n} = 1 - \frac{\mu_{\mathrm{n-1}}\lambda_{\mathrm{n}}}{\mu_{\mathrm{n}}\mu_{\mathrm{n-1}}} \tag{S2}$$

With the surfaces out of contact, a two-layer interferometer was formed, with a layer of solution adjacent to the gel layer. The refractive index μ in Equation S1 was then approximated as a weighted average of the refractive indices of the gel and solution layers,

$$\mu = \frac{h\mu_{\mathrm{gel}} + (D-h)\mu_{\mathrm{sol}}}{D} \tag{S3}$$

where h is the thickness of the gel layer. To measure the wavelengths of the interference fringes for gels of thicknesses greater than 7 µm, a diffraction grating of 1200 grooves/mm was used. For film thicknesses below 7 µm, the large spacing between interference fringes necessitated the use of gratings with 600 grooves/mm and 100 grooves/mm.

Interference fringes were recorded with a camera at 2 frames per second. A MATLAB script was written to determine the pixel locations of pairs of adjacent interference fringes. Gaussian fitting was used to find the pixel location of maximum intensity at the apex of the interference fringes (lowest wavelength), corresponding to the point of closest approach between the silver surfaces. The pixel locations were converted to wavelengths λ_{n} and $\lambda_{\mathrm{n-1}}$ by comparing to the locations of reference wavelengths produced by a mercury lamp. As the surfaces moved, the fringes shifted and eventually left the field of view, at which point the software automatically found a new pair of fringes. The orders of the fringes were determined to greater accuracy by averaging n^{-1} from Equation S2. The average was then inverted and rounded to the nearest whole number. Plotting D as a function of frame number revealed instances where the fringe order calculation was incorrect. In that case, the fringe order was manually incremented or decremented to maintain continuity of D. The fringe order rarely had to be altered by more than one, and most commonly not at all.

Force Measurement

A schematic of the SFA is shown in Figure S2A. The cylinder bearing the gel film was suspended on a double cantilever spring of spring constant $K = 1000$-1200 N/m. The base of the cantilever was translated with a motorized micrometer at constant velocity 10-70 nm/s, corresponding to the initial compression velocity of the surfaces immediately before contact, $\mathrm{d}(d)/\mathrm{d}t|_{d=0}$. As a result of compressing the surfaces with a spring, the compression velocity was less than the initial velocity: $\mathrm{d}(d)/\mathrm{d}t < \mathrm{d}(d)/\mathrm{d}t|_{d=0}$. Velocity was determined from the change in D over time t with the surfaces out of contact, where D varies linearly with t (Figure S2B). The gel film was brought into contact with a bare silver-coated cylindrical glass surface ($R = 2$ cm) in a crossed cylinder configuration, equivalent to a rigid sphere ($R = 2$ cm) compressing a film on a rigid flat substrate.[10] The film was immersed in a capillary meniscus of solution between the surfaces. A solution reservoir in the sealed SFA chamber prevented evaporation of the meniscus. With the surfaces in contact ($D < h$), deviations from linearity of D corresponded to deflections of the spring Δx due to interactions between the surfaces. The normal force F was calculated from the spring deflection via Hooke's law, $F = K\Delta x$. To avoid errors in surface detection,[11] the film thickness h was determined by fitting the poroelastic[12] and Winkler[13] models to the measured forces. The compression depth was calculated as $d = h - D$. The compression velocity was calculated as $\mathrm{d}(d)/\mathrm{d}t = \Delta d/\Delta t$, where Δ indicates the change between adjacent data points ($\Delta t = 0.5$ s). Contact radius a was estimated as the base radius of a spherical cap of radius R and height d, where $a = \sqrt{2Rd}$ for $d \ll R$. Dividing the force by the contact area gives the average pressure $P_{\mathrm{avg}} = F/\pi a^2 = F/2\pi Rd$. The poroelastic[12] and Winkler[13] models give the same expression for the maximum pressure at the center of the contact area: $P_{\mathrm{max}} = 2P_{\mathrm{avg}}$. In all experiments, the maximum pressure was kept below the predicted osmotic pressure of the gel (27 kPa).[14] We assumed that possible changes in polymer concentration due to compression of the gels at these relatively low loads and small strains did not strongly influence the gel elastic modulus. Limiting the maximum pressure also avoided extensive drainage of the gel that would be expected at pressures above the osmotic pressure.[14] Such drainage might correspond to a discontinuous change in compression velocity at high loads which was not observed in our experiments.

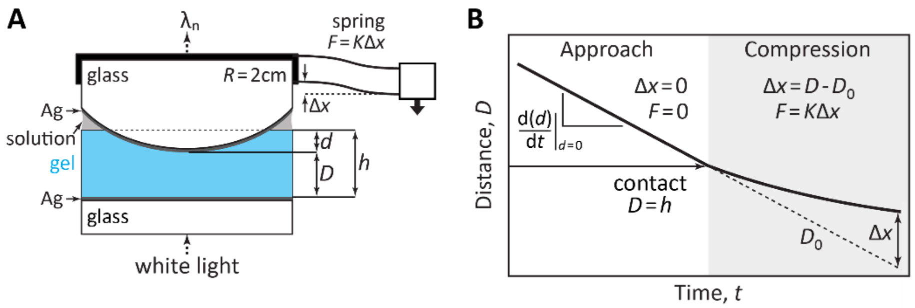

Figure S2. (A) Schematic of a hydrogel film compressed in a surface forces apparatus. For simplicity, the diagram shows a side view of a sphere-on-flat configuration, instead of the true crossed cylinder configuration of the SFA shown in Figure 1B of the main text. The equivalence of the sphere-on-flat and crossed cylinder configurations is shown in section S3 below. The surfaces are shown in compression, and the double cantilever spring is correspondingly deflected by distance Δx. Film thickness h, separation distance D, and compression depth d are indicated. (B) Measurement of initial velocity $\mathrm{d}(d)/\mathrm{d}t|_{d=0}$ and normal force F.

S3. Crossed cylinder force derivation

Consider an isotropic linear elastic film compressed between crossed cylinders, where the axis of the upper cylinder is aligned with the x_1-axis, that of the lower cylinder is aligned with the x_2-axis, and the thickness direction in the film is aligned with the x_3-axis. The film thickness is h and the radius of each cylinder is R. We assume that $h \ll R$ and that the film is much larger than the contact region. The surface of the upper cylinder is given by

$$x_3 = \left(\frac{h}{2} - \frac{d}{2} + R - \sqrt{R^2 - x_2^2}\right) \tag{S4}$$

where d is the distance the film is compressed at the center of the contact region, here called the compression depth. Since $h \ll R$, the surface profile of the cylinder within the contact region can be approximated as a parabola and S4 can be rewritten as

$$x_3 = \left(\frac{h}{2} - \frac{d}{2} + \frac{x_2^2}{2R}\right) \tag{S5}$$

Similarly, the surface of the lower cylinder within the contact region is approximated by

$$x_3 = -\left(\frac{h}{2} - \frac{d}{2} + \frac{x_1^2}{2R}\right) \tag{S6}$$

Adding S5 and S6 yields the distance D between the cylinder surfaces

$$D = h - d + \frac{x_1^2 + x_2^2}{2R} = h - d + \frac{r^2}{2R} \tag{S7}$$

where r is the radial distance from the center of the contact region ($x_1 = x_2 = 0$). At the edge of the contact region, $D = h$, and therefore the radius a of the contact region is

$$a = \sqrt{2Rd} \tag{S8}$$

The strain in the film ε_{ij} at mechanical equilibrium can be expressed as

$$\varepsilon_{ij} = \frac{1}{2}\left(\frac{\partial u_i}{\partial x_j} + \frac{\partial u_j}{\partial x_i}\right) = \frac{1+\nu}{E}\sigma_{ij} - \frac{\nu}{E}\sigma_{kk}\delta_{ij} \tag{S9}$$

where x_i is the position of a material point, u_i is the displacement of a material point, σ_{ij} is the stress in the film, E is the Young's modulus, ν is the Poisson's ratio, and δ_{ij} is the Kronecker delta. Following Johnson,[13] we ignore lateral stress in the film, and assume frictionless compression. With $\sigma_{11} = \sigma_{22} = 0$, Equation S9 gives the following expression for normal stress in the film:

$$\sigma_{33} = E\frac{\partial u_3}{\partial x_3} \tag{S10}$$

The strain in the vertical direction is calculated from Equation S7 as

$$\frac{\partial u_3}{\partial x_3} = \left(-\frac{d}{h} + \frac{r^2}{2hR}\right) \tag{S11}$$

Combining Equations S10 and S11 yields

$$\sigma_{33} = E\left(-\frac{d}{h} + \frac{r^2}{2hR}\right) \tag{S12}$$

The compressive force applied by the cylinders is

$$F = -2\pi \int_0^{\sqrt{2Rd}} r\sigma_{33}\mathrm{d}r = 2\pi E \int_0^{\sqrt{2Rd}} \left(\frac{dr}{h} - \frac{r^3}{2hR}\right)\mathrm{d}r = \frac{\pi R E d^2}{h} \tag{S13}$$

This expression matches the Winkler model derived by Johnson[13] for a sphere compressing a flat gel, and justifies the use of the poroelasticity equation derived by Delavoipière et al. for a sphere-flat geometry[12] (Equation S15).

S4. Theoretical estimation of permeability

For a random isotropic network, the permeability k can be calculated from the characteristic size of the polymer chains a and the solid volume fraction ϕ as follows[15]

$$k = a^2 \frac{3}{20\phi}(-\ln(\phi) - 0.931) \tag{S14}$$

For 7.5 wt% hydrogels, the as-cast volume fraction ϕ_0 can be estimated from the density of water (1 g/ml) and solid polyacrylamide (1.19 g/ml), giving $\phi_0 = 0.064$. From the confocal microscopy images shown in Figure S1B, the gel thickness increases by approximately 64 % due to swelling from thickness 7 to 11.5 µm. We assume that the gels swell in only one dimension due to the glutaraldehyde surface treatment, and therefore that the volume increases 64 %, resulting in a volume fraction $\phi = 0.039$ of the swollen gel. This assumption is supported by the lack of wrinkling observed in Figure S1B and by the swelling study shown in Figure S6. Taking a as the diameter of the polyacrylamide chains (~0.5 nm)[16] yields $k \approx 2$ nm^2.

S5. Poroelastic model and algorithm for force calculation

The poroelastic equation presented here combines Biot Theory and Darcy's law. Biot Theory[17] relates the force compressing a fluid-filled porous material to elasticity and fluid pressure, and Darcy's law relates fluid flow through a porous medium to the pressure gradient. The equations have been previously derived for compression of a gel between parallel plates[18,19] and for a sphere-flat geometry with a thin film approximation.[12] As shown in S3 above, the crossed cylinder geometry is expected to yield the same forces as the sphere-on-flat geometry. For a rigid sphere compressing a thin film on a rigid flat surface, the normal force F can be expressed as

$$F = \frac{\pi R d^2}{h}\left(E + \frac{\eta R}{2k}\frac{\mathrm{d}(d)}{\mathrm{d}t}\right) \tag{S15}$$

where R is the radius of curvature of the sphere, h is the thickness of the gel under zero load, η is the dynamic viscosity of the fluid, k is the permeability of the gel, d is the compression depth, and $\mathrm{d}(d)/\mathrm{d}t$ is the compression velocity. Equation S5 appears in the main text as Equation (1).

For a gel film compressed to a force F_0 and compression depth d_0, if the motor driving the surfaces together is stopped, the surfaces will continue approaching each other until equilibrium is reached and the surfaces stop moving. Because force is applied with a spring, as the surfaces relax and approach each other, the normal force decreases. The normal force therefore depends on the compression depth d as follows:

$$F = F_0 - K(d - d_0) \tag{S16}$$

where K is the spring constant. Equation S5 be rearranged to solve for $\mathrm{d}(d)/\mathrm{d}t$:

$$\mathrm{d}(d)/\mathrm{d}t = \frac{2k}{\eta R}\left(\frac{hF}{\pi R d^2} - E\right) \tag{S17}$$

Combining Equations S6 and S7 yields

$$\mathrm{d}(d)/\mathrm{d}t = \frac{2k}{\eta R}\left(\frac{h(F_0 - K(d - d_0))}{\pi R d^2} - E\right) \tag{S18}$$

which can be fit to the measured $\mathrm{d}(d)/\mathrm{d}t$ as shown in Figure 2C in the main text.

The force needed to compress a thin poroelastic film was also modeled. Driving the base of the cantilever spring at constant velocity $\mathrm{d}(d)/\mathrm{d}t|_{d=0}$ results in the following relationship between force and compression depth:

$$F = K(t\,\mathrm{d}(d)/\mathrm{d}t|_{d=0} - d) \tag{S19}$$

where t is the time since contact ($t = 0$ at $d = 0$). Equation S8 can be written in discrete form and rearranged as:

$$\Delta d = \frac{2k\Delta t}{\eta R}\left(\frac{hK(t\mathrm{d}(d)/\mathrm{d}t|_{d=0} - d)}{\pi R d^2} - E\right) \tag{S20}$$

The compression force F can then be calculated with the following algorithm:

```
Choose $\Delta t$ and tolerance
Set initial values ($i = 0$): $t_0 = 0$, $d_0 = 0$, $F_0 = 0$
For $i = 1$ to $N$ [
    $t_i = t_{\mathrm{i}-1} + \Delta t$
    guess $\Delta d_{\mathrm{i}} = 0$
    $d_i = d_{\mathrm{i}-1} + \Delta d_{\mathrm{i}}$
    Calculate $\Delta d_{\mathrm{i,calc}}$ with Equation S20
    While $|\Delta d_{\mathrm{i,calc}} - \Delta d_{\mathrm{i}}|$ < tolerance {
        Update guess for $\Delta d_{\mathrm{i}}$
        $d_i = d_{\mathrm{i}-1} + \Delta d_{\mathrm{i}}$
        Calculate $\Delta d_{\mathrm{i,calc}}$ with Equation S20
    }
    $\mathrm{d}(d_{\mathrm{i}})/\mathrm{d}t = \frac{d_{\mathrm{i}} - d_{\mathrm{i}-1}}{\Delta t}$
    Calculate $F_i$ with Equation S15
]
```

The guess for Δd_{i} was updated by a factor that progressively decreased until Δd_{i} was within the desired tolerance of $\Delta d_{\mathrm{i,calc}}$. Δt was chosen to be 0.1 s. Tolerance was chosen to be 10^{-6} µm.

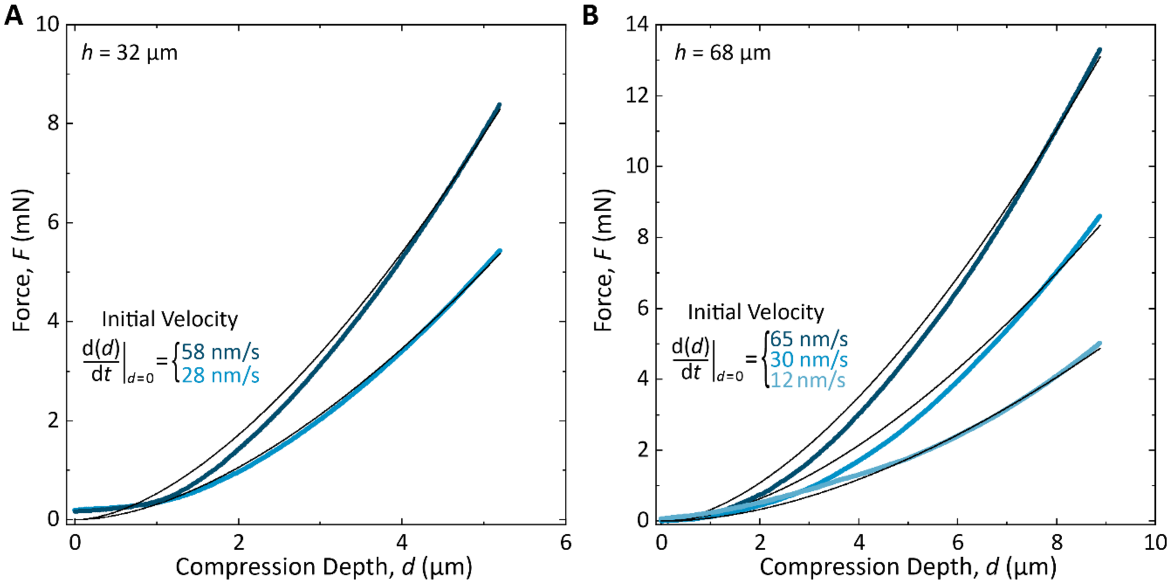

Figure S3. Normal force F vs. compression depth d measured for gel films of different thicknesses compressed at different velocities. (A) Film thickness $h = 32$ µm and (B) $h = 68$ µm. Black curves show the calculations using the poroelastic model. The film thickness h was determined from a one-parameter fit of Equation (S15) to the measured forces, using the measured values of $\mathrm{d}(d)/\mathrm{d}t$. E and k were determined from the relaxation experiments described in the main text. The agreement between the model and the measured forces supports the accuracy of the values of E and k and suggests that the model could calculate compression forces for films of arbitrary thickness provided that the thin-film assumption of the model holds.

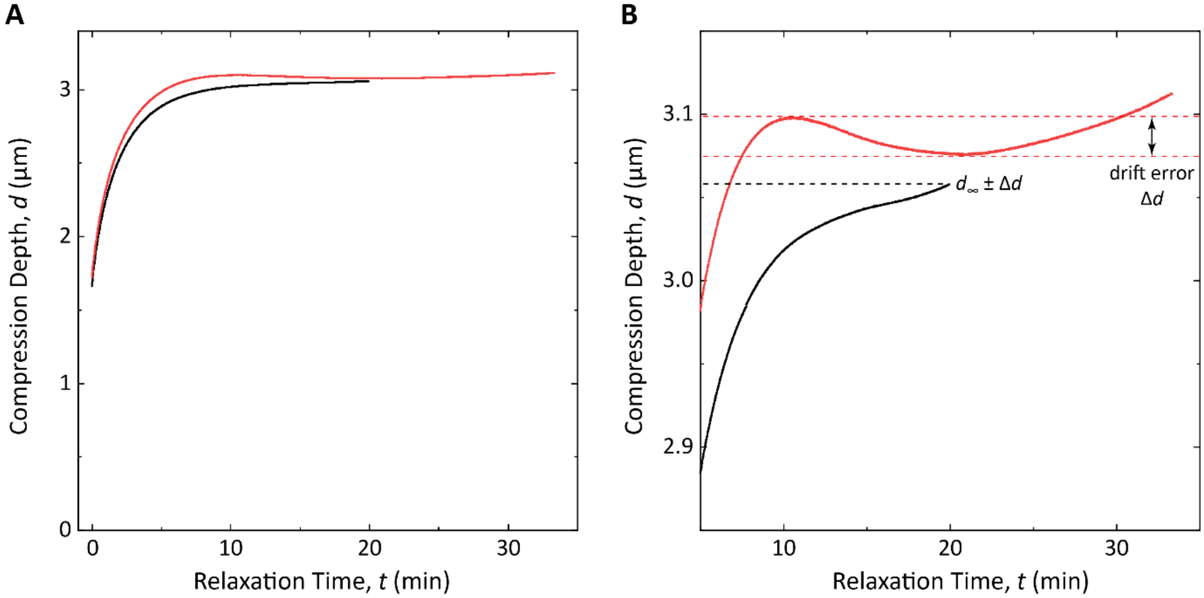

Figure S4. (A) Compression depth d vs. relaxation time t measured during sequential relaxation periods lasting 20 min (black) and 60 min (red). The 60-min relaxation period is truncated. While the 1-, 5-, and 20-min relaxations shown in Figure 2C in the main text follow the same trajectory, the 60-min relaxation reaches larger compression depths more quickly, possibly due to fluid drainage or microstructural changes of the gel occurring during the 20-min relaxation. (B) The data from (A) replotted to show the variations in the limiting value, likely due to thermal drift. The peak-to-peak variation over the first 20 min of the 60-min relaxation was taken as an approximate error of d_∞ for the 20-min relaxation.

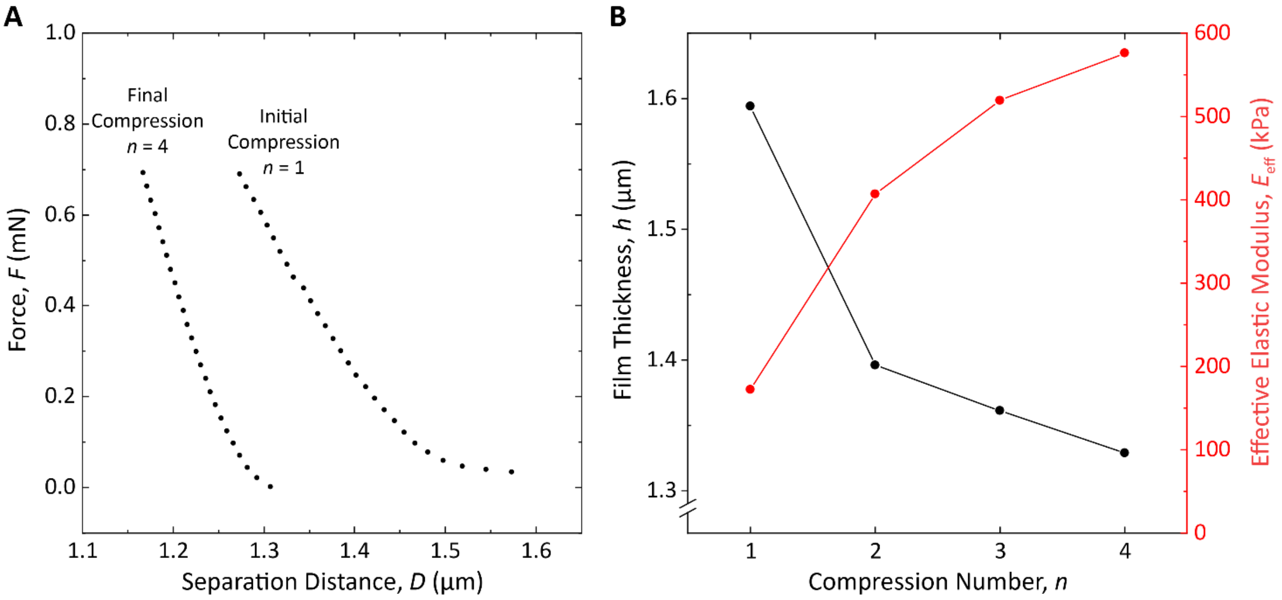

Figure S5. (A) Force F vs. separation distance D measured after addition of 100% ethanol. Four compressions were conducted, where the first ($n = 1$) and last ($n = 4$) are shown. (B) Film thickness h (black circles) and effective modulus E_{eff} (red circles) vs. compression number n. Lines are included to guide the eye.

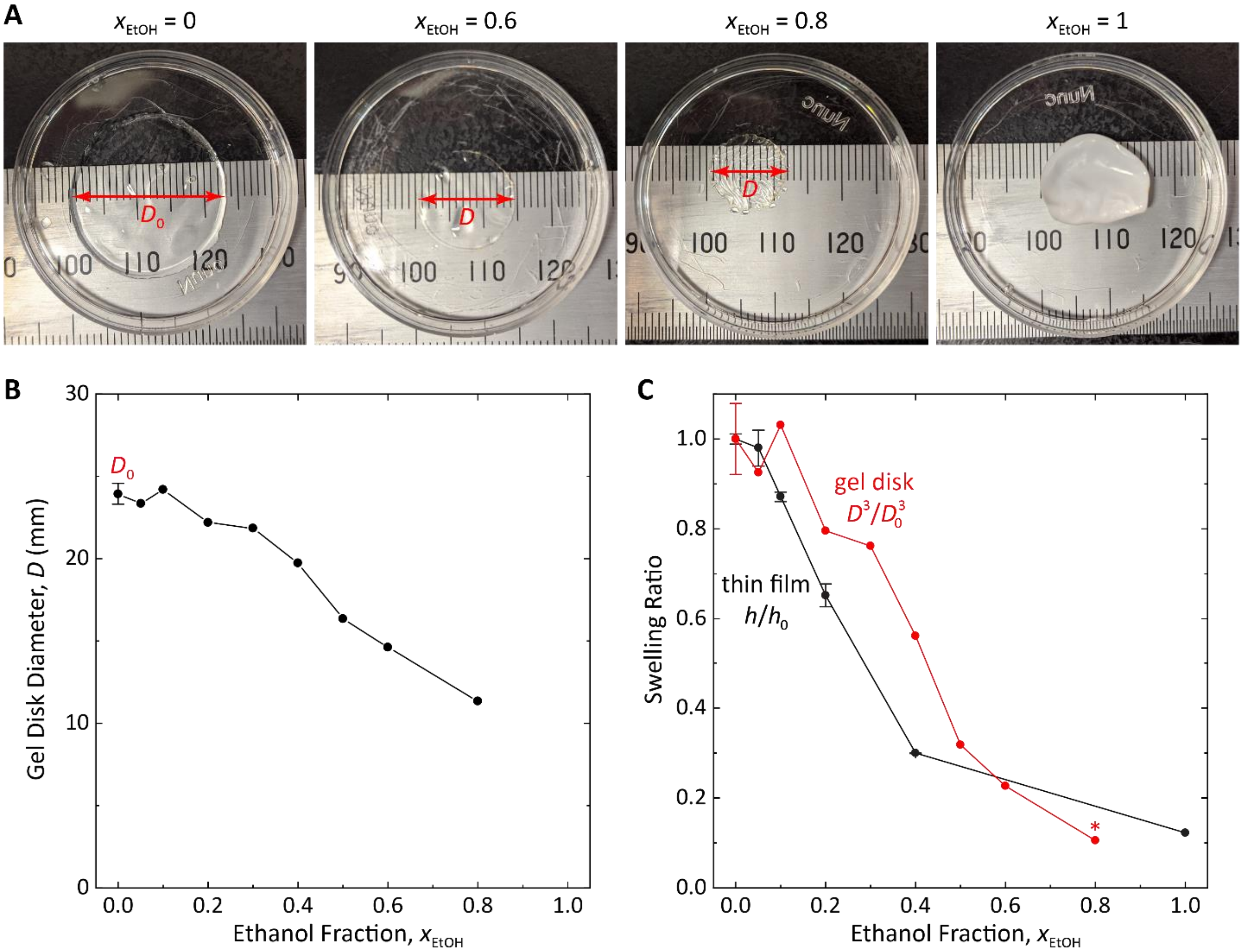

Figure S6. Hydrogel swelling ratios in ethanol solutions. Macroscopic gel disks of as-cast diameter 22 mm were swollen in water for 24 h to an initial swollen diameter D_0. The gels were then immersed in ethanol/water solutions of ethanol fraction x_{EtOH} and equilibrated for 48 h. (A) Images of gel disks equilibrated in different ethanol concentrations ($x_{\mathrm{EtOH}} = 0$, 0.6, 0.8, 1.0. Not shown: $x_{\mathrm{EtOH}} = 0.05$, 0.1, 0.2, 0.3, 0.4, 0.5). (B) Gel disk diameter D vs. x_{EtOH}. (C) Swelling ratio calculated from the ratio of final volume to initial. Since the gels collapse in ethanol, the ratio is less than 1. Red circles show the swelling ratios calculated for the macroscopic gel disks. The disks were unconstrained in the ethanol solutions, and therefore the collapse was assumed to be isotropic for $x_{\mathrm{EtOH}} < 1$, and the swelling ratio was calculated as the ratio of cubed diameter of the disk in ethanol solution to the cubed diameter of the disk in water (D^3/D_0^3). The asterisk for the data point at $x_{\mathrm{EtOH}} = 0.8$ indicates that the value is an underestimate of the swelling ratio, because the wrinkling of the gel shown in (A) lowered the measured value of D. For $x_{\mathrm{EtOH}} = 1$, the collapse occurred within the first minute of immersion, presumably fast enough to result in anisotropic collapse, and the diameter for $x_{\mathrm{EtOH}} = 1$ was not measured. For comparison, black circles show the swelling ratios calculated for a thin gel film from the film thicknesses plotted in the inset of Figure 3A in the main text. As stated in the main text, because the thin gel film was chemically attached to the silver surface, the film was assumed to collapse in only one dimension. Therefore, the swelling ratio for the thin film was calculated from the ratio of the film thickness in ethanol solution to the film thickness in water (h/h_0).

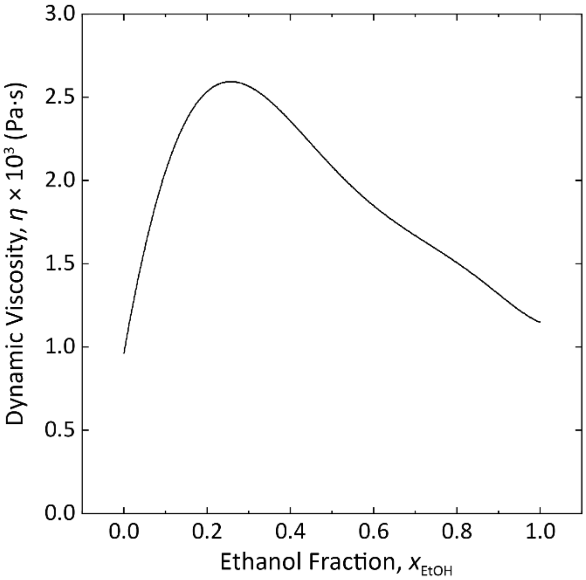

Figure S7. Dynamic viscosity η of ethanol/water solution vs. ethanol fraction x_{EtOH}.[20]

S6. References

1 A. Kudelski and W. Hill, *Langmuir*, 1999, **15**, 3162.
2 A. Michota, A. Kudelski and J. Bukowska, *Langmuir*, 2000, **16**, 10236.
3 Y. Xiao, H. X. Ju and H. Y. Chen, *Anal. Chim. Acta*, 1999, **391**, 73.
4 P. G. de Gennes, *Scaling Concepts in Polymer Physics*; Cornell University Press: Ithaca, NY, 1979.
5 G. Hoch, A. Chauhan and C. J. Radke, *J. Memb. Sci.*, 2003, **214**, 199.
6 R. Tadmor, N. Chen and J. N. Israelachvili, *J. Colloid Interface Sci.*, 2003, **264**, 548.
7 A. M. Hecht and E. Geissler, *J. Phys.*, 1978, **39**, 631.
8 R. Fernandez-Prini and R. B. Dooley, *The International Association for the Properties of Water and Steam*. 1997, pp 1–7.
9 T. A. Scott, *J. Phys. Chem.*, 1946, **50**, 406.
10 J. N. Israelachvili, *Intermolecular and Surface Forces*, 3rd ed.; Academic Press, 2011.
11 J. D. Kaufman and C. M. Klapperich, *J. Mech. Behav. Biomed. Mater.*, 2009, **2**, 312.
12 J. Delavoipière, Y. Tran, E. Verneuil and A. Chateauminois, *Soft Matter*, 2016, **12**, 8049.
13 K. L. Johnson, *Contact Mechanics*; Cambridge University Press: Cambridge, 1985.
14 A. Bhattacharyya, C. O'Bryan, Y. Ni, C. D. Morley, C. R. Taylor and T. E. Angelini, *Biotribology*, 2020, **22**, 100125.
15 G. W. Jackson and D. F. James, *Can. J. Chem. Eng.*, 1986, **64**, 364.
16 H. R. Maurer, *Disc Electrophoresis and Related Techniques of Polyacrylamide Gel Electrophoresis*; De Gruyter: Berlin, 1978.
17 M. A. Biot, *J. Appl. Phys.*, 1941, **12**, 155.
18 C. W. McCutchen, *Wear*, 1962, **5**, 1.
19 G. Cederbaum, L. Li and K. Schulgasser, In *Poroelastic Structures*; Elsevier Science Ltd, 2000; pp 111–134.
20 B. González, N. Calvar, E. Gómez and Á. Domínguez, *J. Chem. Thermodyn.*, 2007, **39**, 1578.